Improved Ordering of Quasi-Two-Dimensional MoS_2 via an Amorphous-to-Crystal Transition Initiated from Amorphous Sulfur-rich $\mathbf{MoS_{2+x}}$

Milos Krbal,[*,†] Vit Prokop,[†] Jan Prikryl,[†] Jhonatan Rodriguez Pereira,[†] Igor Pis,[‡] Alexander V. Kolobov,[¶,§] Paul J. Fons,[§,‖] Yuta Saito,[§] Shogo Hatayama,[§] and Yuji Sutou[⊥,#]

†*Center of Materials and Nanotechnologies (CEMNAT), Faculty of Chemical Technology, University of Pardubice, Legions Square 565, 530 02 Pardubice, Czech Republic*

‡*CNR-IOM, TASC Laboratory, 34149 Basovizza (TS), Italy*

¶*Department of Physical Electronics, Herzen State Pedagogical University of Russia, 48 Moika Emb., St. Petersburg 191186, Russia*

§*Device Technology Research Institute, National Institute of Advanced Industrial Science and Technology, 1-1-1 Umezono, Tsukuba 305-8568, Ibaraki, Japan*

‖*Faculty of Science and Technology, Keio University, Department of Electronics and Electrical Engineering, 223-8522 3-14-1 Hiyoshi, Kohoku-ku, Yokohama, Kanagawa 223-8522, Japan*

⊥*Department of Materials Science, Graduate School of Engineering, Tohoku University, 6-6-11, Aoba-yama, Aoba-ku, Sendai, 980-8579, Japan*

#*WPI Advanced Institute for Materials Research, Tohoku University, 2-1-1 Katahira, Aoba, Sendai 980-8577, Japan*

E-mail: milos.krbal@upce.cz

Phone: +420 466 037 404

*

Abstract

The synthesis of stoichiometric two-dimensional (2D) transition metal dichalcogenides (TMDC) over large areas remains challenging. Using a combination of X-ray diffraction and X-ray absorption spectroscopy, we demonstrate the advantages of using a thin amorphous layer of S-rich MoS_2 (MoS_4 in this paper) for the growth of well-ordered crystalline MoS_2 films by annealing at 900 °C. In contrast to the crystallization of stoichiometric amorphous MoS_2 , crystallization of the as-deposited amorphous MoS_4 phase shows strong preferred ordering of layered MoS_2 on a Si/SiO_x non-templating substrate with the [002] crystallographic plane dominant and accompanied by Kiessig fringes indicating the improved crystallinity of the MoS_2 layers. A similar effect can be only achieved by templated crystallization of an amorphous MoS_2 thin film deposited on a c-plane sapphire substrate. We suggest that the crystal growth improvement originates from the lower coordination number (CN) of the Mo atoms in the MoS_4 amorphous phase (CN = 4) in comparison with the CN = 6 of amorphous MoS_2 and the gradual release of free sulfur atoms from the thin film during crystallization.

Keywords: Thin films; X-ray absorption spectroscopy; MoS_2; local structure; crystallization; molecular dynamics; optical properties; XPS

Introduction

Two-dimensional (2D) transition metal dichalcogenides (TMDC) have demonstrated a very strong application potential in many areas depending on the form of the crystalline phase. Flat, large single-layer crystals have been used for fabrication of optoelectronics and sensors,[1–3] while standing flakes, nanoparticles or thin films have shown their potential in applications such as photocurrent generation,[4–6] photocatalytic degradation of organic pollutants,[7,8] electrocatalytic evolution of hydrogen[9–11] and energy[10,12] or data storage.[13,14] An urgent task in the application of TMDCs is therefore the development of synthesis techniques for the growth of well-defined crystals with a controlled number of layers over large areas.

A number of processes have been proposed to prepare the desired sizes and orientation of TMDC layers.[2,10,15,16] Exfoliation of chalcogenide single crystals with a van der Waals gap is a widely used top-down method of preparing chalcogenide monolayers to obtain layers in the form of small flakes with sizes typically on the order of a few μm. In contrast, bottom-up growth technology utilizes the transformation of precursors by physical and chemical processes. Currently, chemical vapor deposition (CVD) is one of the most widely used bottom-up techniques for TMDC synthesis. Using this strategy, various 2D TMDCs can be easily grown over large areas on different substrates, which determine both the size and shape of the prepared monolayer crystals.[17] Although the crystalline planes exhibit strong out of plane orientation with crystallites mostly triangular in shape, the in-plane orientation tends to be random making conformal coverage of entire substrate surface challenging. Atomic layer deposition (ALD), for example, can successfully coat a large surface area of nanostructures with a high aspect ratio (a length : diameter ratio) using vertically oriented flakes of TMDCs with a typical size of several nm,[18,19] allowing the creation of a high density of active centers for catalytic applications. However, the necessity of the use of very toxic organic and/or inorganic precursors in conjunction with the proper deposition conditions are critical disadvantages of this technique.

Nearly perfect surface coverage over a large substrate area can be achieved by either thermal decomposition of dipped or spin-coated $(NH_4)_2Mo(W)S_4$ under an inert or sulfur atmosphere[20,21] or using near equilibrium physical vapour deposition techniques.[22,23] Due to the large differences in vapour pressure among the constituent elements, the desired composition can be ensured by reactive deposition under a H_2S atmosphere with substate temperatures above 400 °C,[24] which results in the desorption of excess sulphur from the film. Since thio-compounds can only be used and H_2Se and H_2Te gases are toxic and even unstable at elevated temperature, both approaches are strictly limited to the preparation of transition metal disulphides. Therefore, two-step bottom-up processes were developed as an alternative path for the fabrication of crystalline TMDCs. In principle, they include deposition of a

thin film of a transition metal[25] or a transition metal oxide[26] on a substrate in the first step and subsequent conversion of this layer to a TMDC in a vapour of chalcogen or the formation of layered crystalline phase via transformation from a 3D continuous amorphous phase as has been very recently demonstrated for $MoTe_2$[27] and MoS_2.[28] In the latter study, it was reported that an amorphous MoS_2 thin film crystallized with a strong [002] preferred orientation even on non-templating substrates and its conversion to the 2H layered phase was shown to proceed via the 1T' phase as disclosed by means of *ab initio* molecular dynamics simulations. To date, only the transformation of a stoichiometric amorphous phase has been considered. In general, the composition of the amorphous phases can be easily tuned by deposition conditions and thus non-stoichiometric compositions of amorphous phases can be utilized. Because the amorphous phase crystallizes in a stoichiometric composition with the general formula MX_2 and excess chalcogen can be desorbed from the film during the transformation process due to its large vapour pressure, chalcogen-rich amorphous phases may provide an essential platform for improving crystal order.

In this paper, we investigate the role of sulfur content on the amorphous-to-crystal (or 3D-2D) transformation starting from stoichiometric amorphous MoS_2 and S-rich amorphous MoS_4 , and examine both long- and short-range order. Using a combination of X-ray diffraction and X-ray absorption spectroscopy, we demonstrate the advantages of the use of amorphous S-rich MoS_4 for the production of well-ordered crystalline MoS_2 films by crystallization of a thin amorphous layer by annealing at 900 °C. In contrast to crystalline films produced from stoichiometric amorphous MoS_2 , crystallization of the as-deposited amorphous MoS_4 phase shows strong [002] preferred crystal growth of layered MoS_2 on a Si/SiO_x non-templating substrate along with Kiessig fringes indicating improved ordering of the MoS_2 layers. A similar effect can be only achieved by templated crystallization of an amorphous MoS_2 thin film deposited on a c-plane oriented sapphire substrate.The proposed approach demonstrates a simple and efficient way to fabricate well-ordered thin 2D TMDCs even on non-templating substrates for applications in nano- and optoelectronic devices.

Experimental details

Amorphous MoS_2 and MoS_4 thin films were deposited at room temperature by pulsed laser deposition in an off-axis geometry using a KrF laser with a wavelength of 248 nm and the pulse length of 30 ns. The distance between the MoS_2 target and the substrate holder was $\approx$ 4 cm. For deposition of the amorphous thin films, the laser frequency was set to 1 Hz while the laser output intensities of 0.5 J/cm^2 and 21 J/cm^2 were used to grow amorphous films with the compositions MoS_4 and MoS_2 , respectively. All depositions were performed with a base pressure of 2.8×10^{-4} Pa. A [100] silicon wafer covered with a native oxide layer was used as a substrate. The thickness of the as-deposited films was about 50 nm, which corresponds to about 1500 pulses. Prior to opening the chamber, the deposited samples remained under vacuum for an additional 2 hours to allow the samples to cool and release stress.

Amorphous MoS_2 films were deposited at room temperature using magnetron sputtering onto a silicon/SiO_x wafer and sapphire substrates with c- and a- surface orientations. The thickness of the as-deposited films was about 50 nm.

To prevent sample oxidation during crystallization, samples ware placed into a clean quartz ampoule which was subsequently evacuated to 10^{-3} Pa and sealed. The crystallization process was carried out in a furnace with a heating rate of 2 °C/ min, with heating at temperatures ranging from $100 - 900\,^{\circ}$C for one hour and which they were allow to cool down to room temperature naturally.

X-ray diffraction measurements were carried out on both amorphous and crystalline samples of MoS_2 and MoS_4 , using a diffractometer (Empyrean Malvern Panalytical) operated in two-theta/omega mode to fully satisfy the Bragg-Brentano geometry.

Surface compositional analyses were carried out by X-ray photoelectron spectroscopy (XPS, ESCA2SR, Scienta-Omicron) using a monochromatic Al Kα (1486.7 eV) X-ray source. The binding energy scale was calibrated to the carbon peak at 284.8 eV. The spectra were fit using Shirley-type background and Voigt line-shapes. The S 2p and Mo 3d peak doublet

separation and intensity ratios were calibrated on a MoS_2 powder reference sample.

Mo K-edge X-ray absorption spectra (XAS) for the as-deposited and crystalline samples were measured in fluorescence mode using grazing incidence geometry at beamline BL01B1 at SPring-8. XAS data were processed and fitted using the Athena and Arthemis software packages.[29]

Results and discussion

Figure 1 A and B shows the evolution of XRD patterns during the transformation of the amorphous MoS_2 and MoS_4 thin films, respectively, into the crystalline MoS_2 phase by ex-situ annealing up to 900 °C. It is obvious from figure 1 that albeit both amorphous phases crystallize in the 2H layered phase of MoS_2 with a strong preferred [002] out-of-plane c-axis orientation,[30] the onset of the phase transformation in MoS_4 appears at 700 °C, a value almost about 200 °C lower than that of stoichiometric amorphous MoS_2 . Additional Bragg reflections, the [006] and [008], of crystalline MoS_2 were present in XRD pattern of crystalline MoS_2 originating from MoS_4 , which indicates the ordering of the two-dimensional layers into a well-crystallized multilayer MoS_2 phase. Focusing on the first diffraction peak along the [002] direction of 2H-MoS_2 prepared from both amorphous phases annealed at 900 °C shown in figure 1C, at first glance, it is clear that the reflection peak of 2H-MoS_2 originating from the amorphous MoS_4 is more intense, narrower and shifted to higher 2θ values in comparison with the same phase grown from stoichiometric amorphous MoS_2 . Furthermore, the Bragg reflection peak is unexpectedly accompanied by Kiessig fringes[31] due to interference from the surface of the layer and the layer/substrate interface. The presence of these satellites equivocally underscores the presence of a ordered 2H-MoS_2 phase with strong out-of-plane c-axis orientation formed by crystallization of amorphous MoS_4 .

Under the assumption that even higher crystal order could be achieved by templated crystallization[32] of an amorphous MoS_2 thin film, we deposited a 50 nm thick amorphous

MoS_2 film (by magnetron sputtering) on a c-axis oriented sapphire substrate, which is expected to strongly promote the growth of the 2H-MoS_2 phase in a given direction and at the same time on an a-axis oriented sapphire as well as Si/SiO_x substrates whose surface is expected not to support the growth of 2H-MoS_2 crystals with the same out-of-plane c-axis orientation. As anticipated, Figure 1D shows that a similar XRD pattern observed after crystallization of MoS_4 in terms of the increased Bragg peak intensity as well as the presence of satellite reflections can be only reproduced by the templated crystallization of an amorphous MoS_2 thin film deposited on c-axis oriented sapphire. On the other hand, the use of non-templated substrates does not affect the ordering in the 2H-MoS_2 crystals because the corresponding XRD patterns do not differ significantly from each other.

Complementary local structural information to the XRD results was obtained by X-ray Absorption Spectroscopy (XAS), which provides information on electronic transitions around the X-ray absorption Mo:K-edge represented by X-ray Absorption Near Edge Spectroscopy (XANES) spectra as well as the coordination numbers and bond lengths. Figure 2 compares the Mo:K-edge XANES spectra of amorphous (A) and crystalline (B) MoS_2 and MoS_4 and their corresponding Fourier transformed Extended X-ray Absorption Fine Structure (EXAFS) data (C-F) including the relevant fitting curves. Comparing the Mo:K-edge XANES spectra of both amorphous phases, it can be seen that the absorption edge for MoS_4 shifts to lower X-ray photon energy by 3 eV and the oscillations above the absorption edge are less pronounced, indicating a difference in the local structure of the two amorphous phases. On the other hand, the Mo:K-edge XANES spectra for both crystallized MoS_2 are very similar, corroborating that the final products of both amorphous phases after their crystallization are the same structure.[28,33] However, a detailed comparison disclosed that the intensity of the so-called white-line is lower for crystallized MoS_2 originating from amorphous MoS_2 as well as that the overall shape of the XANES spectrum is more rounded in contrast to the counterpart XANES spectrum originating from MoS_4 , suggesting that the former structure is less ordered. The results of the real-space fitting of the EXAFS data for amorphous and

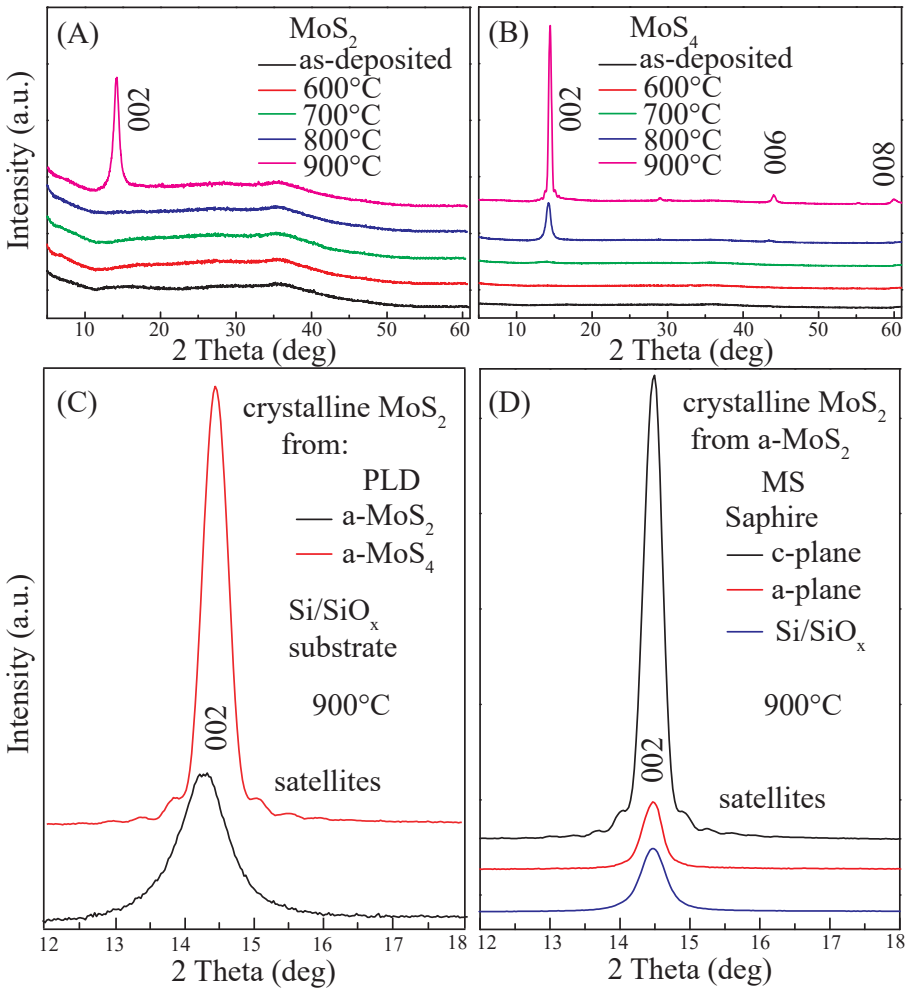

Figure 1: (Color online) XRD patterns of the as-deposited (A) MoS_2 and (B) MoS_4 and both compositions crystallized in the range of temperatures from 600 to 900 °C with a step of 100 °C. (C) zoomed XRD patterns near the [002] reflection of crystallized MoS_2 at 900 °C grown from amorphous MoS_2 and MoS_4 grown by pulsed laser deposition (PLD). (D) zoomed XRD pattern near the [002] reflection of crystallized MoS_2 at 900 °C grown from amorphous MoS_2 and deposited on sapphire (c- and a-plane) and Si/SiO_x substrates grown by magnetron sputtering (MS).

crystalline phases are summarized in Table 1. Focusing on the local structure of both amorphous phases shown in Figure 2 C and E, we found that the first coordination shells around the Mo atoms in both as-deposited MoS_2 and MoS_4 include S and Mo with first-nearest neighbours located at distances of about 2.41 Å and 2.8 Å, respectively. While bond lengths are the same in both amorphous phases, the analysis further reveals that partial coordination numbers of both Mo-S and Mo-Mo bonds differ significantly. The obtained values are 5.11, 1.56 and 2.56, 0.83 for as-deposited amorphous MoS_2 and MoS_4 , respectively, clearly demonstrating that the total coordination numbers for the Mo atom are roughly 6 and 4 in the case of amorphous MoS_2 and MoS_4 , respectively. Our results are in good agreement with recent reports.[34,35] The lower total coordination number of Mo atoms in amorphous MoS_4 explains the lower magnitude of oscillations on the corresponding XANES spectrum and possibly the shift of the absorption edge to lower X-ray photon energy, which is usually associated with the formal oxidation state of the absorbing species. Note the Mo-O bonds are near the detection limit but their contribution noticeably improves the quality of the final fit.

The first coordination shell of both crystallized MoS_2 phases is, on the other hand, exclusively formed by the heteropolar Mo-S bonds with identical bond lengths of 2.41 Å and the second nearest distance is represented by Mo atoms with an interatomic distance of approximately 3.15 Å , which confirms the formation the 2H phase after crystallization. These values are in line with previously reported results.[28,33,36,37] The coordination numbers of the first (Mo-S) and second (Mo-Mo) coordination shells are 5.90, 4.19 and 6.29, 7.67 for crystallized MoS_2 originating from MoS_2 and MoS_4 , respectively, leading to the conclusion that the crystalline MoS_2 phase beginning from MoS_4 is clearly better ordered. We would like to emphasize that the conclusion from the EXAFS experiment is in excellent agreement with the XRD analysis.

To reveal the role of sulfur excess on crystallization, we performed an XPS analysis of as-deposited and crystallized MoS_4 and MoS_2 at 900 °C. Figure 3 A and B show the Mo 3d core

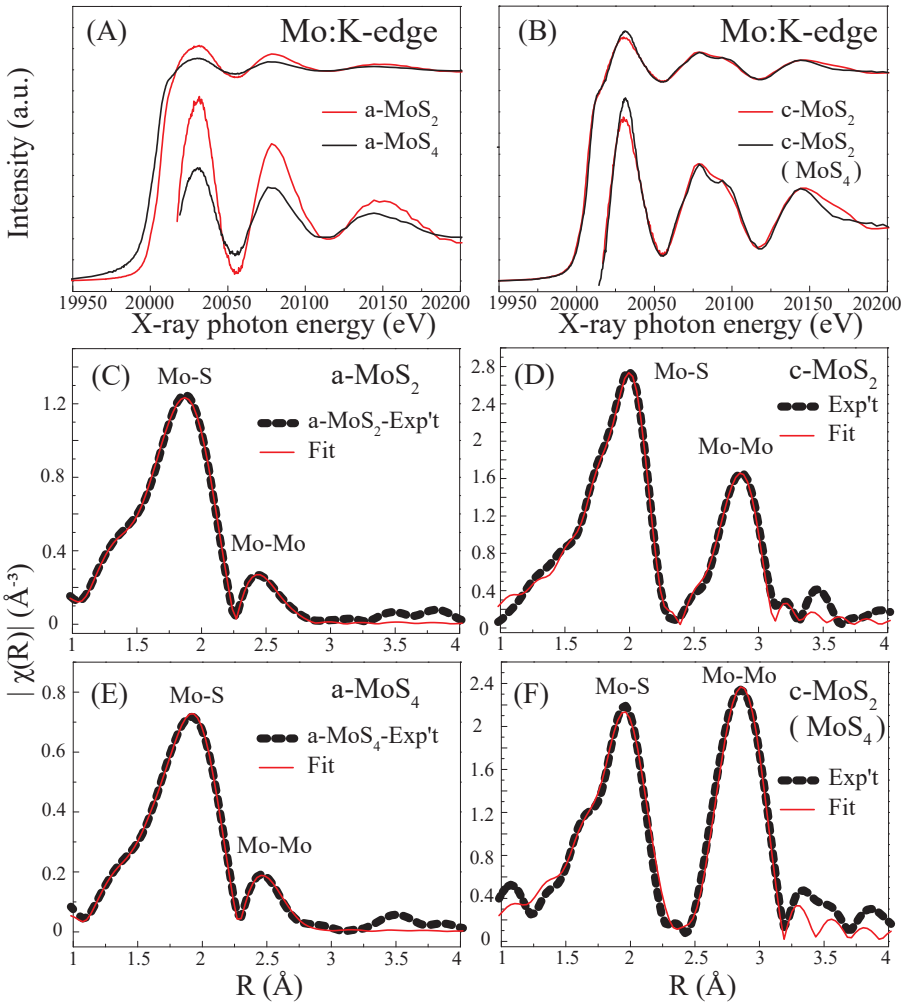

Figure 2: (Color online) Experimental Mo:K-edge XANES spectra of (A) as-deposited amorphous MoS_2 and MoS_4 and (B) MoS_2 crystallized at 900 °C starting from amorphous MoS_2 and MoS_4 . The lower curves show zoomed-in Mo:K-edge XANES spectra above the absorption edge. Real-space fitting of EXAFS data of as-deposited amorphous (C) MoS_2 and (E) MoS_4 and (D and F) corresponding crystallized MoS_2 at 900 °C.

Table 1: Coordination numbers (CN) and bond lengths (BL) of as-deposited and crystallized MoS_4 and MoS_2

	CN	BL/Å
a-MoS_4		
aMo-S	2.56 ± 0.12	2.43 ± 0.01
aMo-Mo	0.83 ± 0.21	2.8 ± 0.02
aMo-O	0.08 ± 0.07	1.57 ± 0.08
a-MoS_2		
aMo-S	5.11 ± 0.22	2.41 ± 0.01
aMo-Mo	1.56 ± 0.39	2.8 ± 0.02
aMo-O	0.37 ± 0.23	1.57 ± 0.02
c-MoS_2 from a-MoS_4		
cMo-S	6.29 ± 0.5	2.41 ± 0.01
cMo-Mo	7.67 ± 0.93	3.18 ± 0.01
c-MoS_2 from a-MoS_2		
cMo-S	5.90 ± 0.27	2.41 ± 0.01
cMo-Mo	4.19 ± 0.61	3.15 ± 0.01
c-MoS_2, the ideal 2H phase[30]		
cMo-S	6	2.37
cMo-Mo	6	3.16

level for as-deposited amorphous MoS_2 and MoS_4 . As recently reported,[28] the Mo 3d core level spectra of both amorphous phases contain a mixture of four doublets attributable to Mo(IV)-S in 1T' - like phase (magenta) containing Mo-Mo homopolar bonds with the binding energy, $E_B(3d_{5/2}) = 228.8$ eV,[9,38] Mo(IV)-S in 2H - like symmetry (light blue) with $E_B(3d_{5/2}) = 229.3$ eV,[38] a weak signal attributable to Mo(VI)-O in MoO_3 (green) with $E_B(3d_{5/2}) = 232.4$ eV[39] and molybdenum oxo-sulphides Mo(IV)-O/S or Mo(V) (brown) with $E_B(3d_{5/2}) = 230.3$ eV.[40,41] Broad bands at $E_B(2s) = 226.3$ eV and $E_B(2s) = 227.4$ eV are attributable to S(II-)[9] and $(S)_n$(II-),[9] respectively. Comparison of Mo 3d core levels of both as-deposited amorphous phases clearly reveals a difference in Mo(IV)-S in 1T' - like : Mo(IV)-S in 2H - like structural units ratio, which is mainly due to a significant decrease in Mo(IV)-O/S or Mo(V) as a result of Mo(IV)-S in 2H - like unit formation in the case of amorphous MoS_4 . As expected, amorphous MoS_4 contains more polysulfide units than amorphous MoS_2 , as shown by the greater contribution of these units by a S 2s analysis.

Although the results from the Mo 3d and EXAFS core levels of the amorphous phases

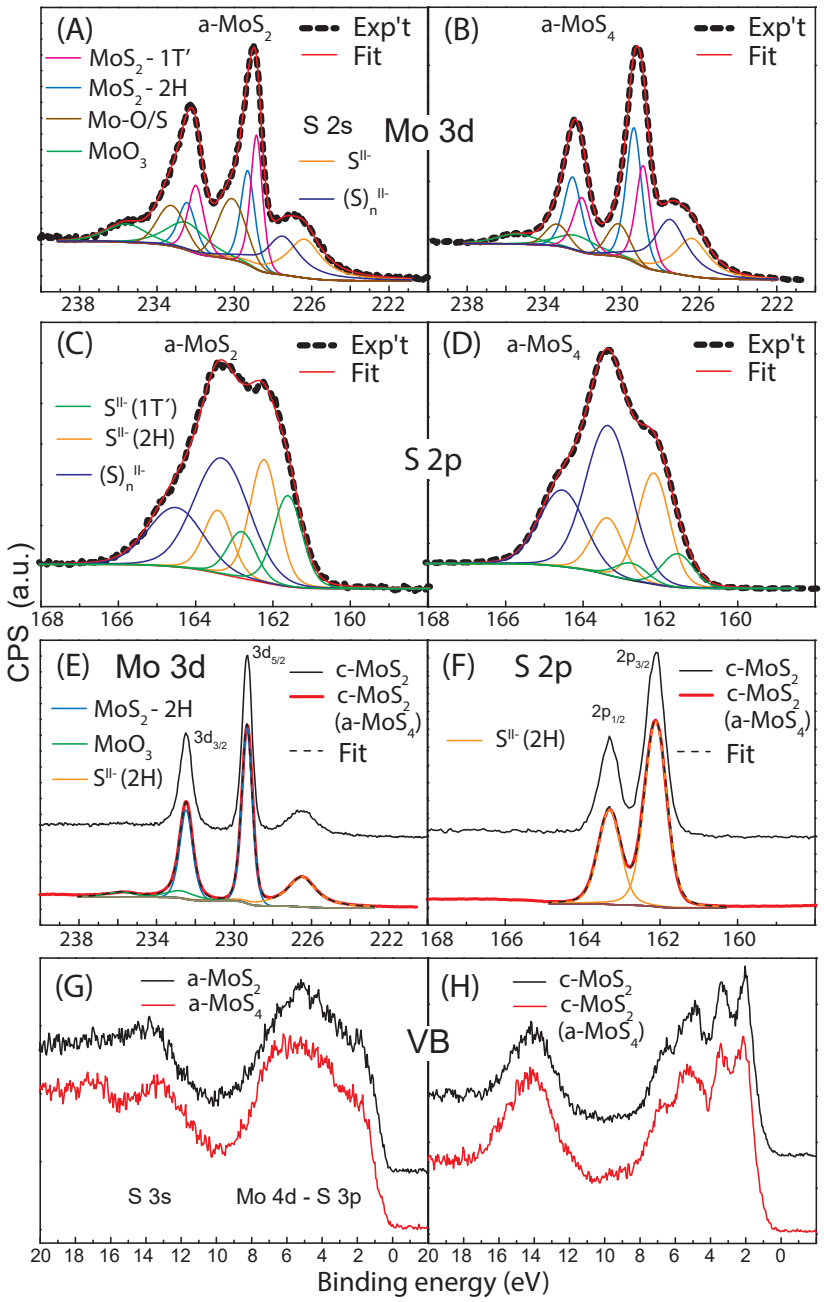

Figure 3: (Color online) The XPS spectra of the as-deposited MoS_2 and MoS_4 (A-D) and crystalline (E,F) MoS_2 . Figures (G, H) demonstrate corresponding valence band spectra.

are mutually supportive, the S 2p analysis provides the missing information on the sulfur arrangement. Analysis of the S 2p core level identified three contributed doublets in both amorphous phases, namely S(-II) in 1T' - like phase (green) with the binding energy, $E_B(2p_{3/2})$ = 161.62 eV,[9,42–44] S(-II) in 2H - like phase (orange) with the binding energy, $E_B(2p_{3/2})$ = 162.24 eV[9] and S_n(-II) with $E_B(2p_{3/2})$ = 162-164 eV assigned to polysulphides with a variable number of sulfur atoms in the chain.[45] At first glance, amorphous MoS_4 contains more S-S bonds compared to amorphous MoS_2 . A significant excess of S atoms in the amorphous phase could therefore play a key role in the improved ordering of layers in the crystalline MoS_2 phase.

On the other hand, after crystallization of both amorphous phases at 900 °C for 1h, the Mo 3d and S 2p core levels are characterized exclusively by Mo(IV)-S and S(-II) oxidation states with 2H symmetry, which demonstrates the presence of a single crystalline phase of MoS_2 . The percentage contributions of the Mo and S oxidation states in all studied phases are summarized in Table 2.

Table 2: Contribution in % of individual components to the XPS signal of as-deposited MoS_2 and MoS_4 and corresponding crystallized MoS_2 . The relative contributions are calculated from integrated intensities after the normalization to corresponding Mo 3d and S 2p sensitivity factors.

Sample	Mo-S (1T'-like)	Mo-S (2H-like)	Mo-O/S	MoO_3	S-Mo	S_n(-II)
aMoS_2	9	7.5	9	6.4	33.9	34.2
cMoS_2	-	31.2	-	3.5	65	-
aMoS_4	7.6	10.7	3.6	3.2	30.5	44.5
cMoS_2	-	29.7	-	3.7	66.3	-

Differences between amorphous MoS_4 and MoS_2 can also be observed by comparison of their valence band (VB) spectra. The binding energy range 0 - 10 eV[46] is characterized by the hybridization of Mo 4d and S 3p. While VB edges of both amorphous phases appear at the same binding energy, The VB of amorphous MoS_4 has a more intense band above 6 eV compared to amorphous MoS_2 . The VB spectra of the corresponding crystalline phases do not differ significantly, indicating the same crystalline phase remains after crystallization.

Our results clearly reveal the connection between the composition of the amorphous Mo-S

phase and the use of substrate orientation on the improved preferential ordering of the 2H layered MoS_2 phase after the amorphous-to-crystal phase transformation. It is well known that the use of a template greatly reduces the nucleation energy. Subsequent crystal growth proceeds "epitaxially" provided that the lattice constants of the template and the grown material do not differ significantly. However, the origin of the observed transformation of three-dimensional amorphous S-rich MoS_4 into a well-ordered 2H-MoS_2 layered structure grown on non-templated substrates seems to be an intrinsic property of TMDC. In light of the obtained results, we believe that the perfect layer-by-layer growth of the MoS_2 crystals starting from amorphous MoS_4 may result from the lower coordination number of the Mo atoms along with a gradual release of the S atoms from the layer during crystallization, which probably offer the higher degree of freedom for Mo-S structural units to be organized into the well-ordered 2H-MoS_2 phase. We would like to note that a similar perfect layer-by-layer growth of the 2H-MoS_2 crystals has been recently observed by sulfurization of a MoO_3 layer.[47] Therefore, we suppose that the change in the local environment of Mo atoms supports nearly perfect layer-by-layer growth and at the same time suppresses for the formation of lamellar structures (crystallites with random orientation).

Conclusion

To conclude, we have demonstrated the advantages of the use of amorphous S-rich MoS_4 for the production of well-ordered crystalline MoS_2 films by means of an amorphous-to-crystal (or 3D-2D) transformation of a thin amorphous layer by annealing at 900 °C. Unlike the case for amorphous stoichiometric MoS_2 , crystallization of the as-deposited amorphous MoS_4 phase resulted in strong layer-by-layer preferred crystal growth of MoS_2 even on a Si/SiO_x non-templating substrate with only the [002] reflections present accompanied by Kiessig fringes indicating the improved ordering of MoS_2 layers. We demonstrated that a similar effect could be only achieved by templated crystallization of an amorphous MoS_2 thin film

deposited on c-plane sapphire substrate. We suggest that the observed improved ordering in MoS_2 crystals starting from amorphous MoS_4 originates from the lower coordination number of the Mo atoms (CN=4 instead of 6) along with a gradual release of the S atoms from the layer during crystallization, which allow the arrangement of Mo-S structural units into the well-ordered 2H-MoS_2 phase. The proposed approach demonstrates a simple and efficient way to fabricate well-ordered thin 2D TMDCs even on non-templating substrates for applications in nano- and optoelectronic devices.

Acknowledgment

This work was supported by the Czech Science Foundation (19-17997S), the Ministry of Education, Youth and Sports (LM2018103), the Russian Foundation for Basic Research [grant RFBR 19-07-00353 (study of the amorphous phase) and a joint RFBR-JSPS project supported by grants RFBR 20-52-50012 and JPJSBP120204815 (3D-2D crystallization)]) and JSPS KAKENHI Grant Number 19H02619. XAS experiments were performed within 2019B1324 SPring8 proposals. I.P. acknowledges funding from the EUROFEL project (RoadMap Esfri).

Author contributions

M.K., A.V.K. and P.F. conceived and designed the experiments. M.K. wrote the manuscript, measured XRD data, analysed EXAFS data. V.P. was responsible for the sample deposition. J.P. analysed XRD data. J.R.-P. carried out the XPS measurement. A.V.K., P.F., Y.Sa., S.Hat., and Y.Su. measured Mo K-edge EXAFS data and I.P. analysed XPS data. A.V.K and P.F. helped with writing the manuscript. All authors discussed the results and commented on the manuscript.

Competing Interests statement

The authors declare that there are no competing interests.

References

(1) Wang, Q. H.; Kalantar-Zadeh, K.; Kis, A.; Coleman, J. N.; Strano, M. S. Electronics and optoelectronics of two-dimensional transition metal dichalcogenides. *Nat Nanotechnol.* **2012**, *7*, 699–712.

(2) Kolobov, A. V.; Tominaga, J. *Two-dimensional Transition-Metal Dichalcogenides*; Springer Series in Materials Science, Springer International Publishing AG, 2016.

(3) Vutukuru, M.; Ardekani, H.; Chen, Z.; Wilmington, R. L.; Gundogdu, K.; Swan, A. K. Enhanced Dielectric Screening and Photoluminescence from Nanopillar-Strained MoS_2 Nanosheets: Implications for Strain Funneling in Optoelectronic Applications. *ACS Appl. Nano Mater.* **2021**, *4*, 8101–8107.

(4) Piper, J. R.; Fan, S. Broadband Absorption Enhancement in Solar Cells with an Atomically Thin Active Layer. *ACS Photonics* **2016**, *3*, 571–577.

(5) Sumesh, C. K. Towards efficient photon management in nanostructured solar cells: Role of 2D layered transition metal dichalcogenide semiconductors. *Solar Energy Materials and Solar Cells* **2019**, *192*, 16–23.

(6) Setayeshmehr, K.; Hashemi, M.; Ansari, N. Photoconversion efficiency in atomically thin TMDC-based heterostructures. *Opt. Express* **2021**, *29*, 32910–32921.

(7) Peng, W.-c.; Li, X.-y. Synthesis of MoS_2/g-C_3N_4 as a solar light-responsive photocatalyst for organic degradation. *Catal. Commun.* **2014**, *49*, 63–67.

(8) Mittal, H.; Khanuja, M. Optimization of $MoSe_2$ nanostructure by surface modification using conducting polymer for degradation of cationic and anionic dye: Photocatalysis

mechanism, reaction kinetics and intermediate product study. *Dyes Pigm* **2020**, *175*, 108109.

(9) Xie, J.; Zhang, H.; Li, S.; Wang, R.; Sun, X.; Zhou, M.; Zhou, J.; Wen, X.; Lou, D.; Xie, Y. Defect-Rich MoS_2 Ultrathin Nanosheets with Additional Active Edge Sites for Enhanced Electrocatalytic Hydrogen Evolution. *Adv. Mater.* **2013**, *25*, 5807–5813.

(10) Eftekhari, A. Molybdenum diselenide ($MoSe_2$) for energy storage, catalysis, and optoelectronics. *Appl. Mater. Today* **2017**, *8*, 1–17.

(11) Pataniya, P. M.; Late, D.; Sumesh, C. K. Photosensitive WS_2/ZnO Nano-Heterostructure-Based Electrocatalysts for Hydrogen Evolution Reaction. *ACS Appl. Energy Mater.* **2021**, *4*, 755–762.

(12) Pomerantseva, E.; Gogotsi, Y. Two-dimensional heterostructures for energy storage. *Nature Energy* **2017**, *2*, 17089.

(13) Hou, X.; Chen, H.; Zhang, Z.; Wang, S.; Zhou, P. 2D Atomic Crystals: A Promising Solution for Next-Generation Data Storage. *Advanced Electronic Materials* **2019**, *5*, 1800944.

(14) Wu, J.; Chen, H.-Y.; Yang, N.; Cao, J.; Yan, X.; Liu, F.; Sun, Q.; Ling, X.; Guo, J.; Wang, H. High tunnelling electroresistance in a ferroelectric van der Waals heterojunction via giant barrier height modulation. *Nature Electronics* **2020**, *3*, 466–472.

(15) Krbal, M.; Prikryl, J.; Zazpe, R.; Dvorak, F.; Bures, F.; Macak, J. M. 2D $MoSe_2$ Structures Prepared by Atomic Layer Deposition. *Phys. Status Solidi Rapid Res. Lett.* **2017**, *12*, 1800023.

(16) Mattinen, M.; Leskelä, M.; Ritala, M. Atomic Layer Deposition of 2D Metal Dichalcogenides for Electronics, Catalysis, Energy Storage, and Beyond. *Adv. Mater. Interfaces* **2021**, *8*, 2001677.

(17) Wang, J.; Li, T.; Wang, Q.; Wang, W.; Shi, R.; Wang, N.; Amini, A.; Cheng, C. Controlled growth of atomically thin transition metal dichalcogenides via chemical vapor deposition method. *Materials Today Advances* **2020**, *8*, 100098.

(18) Motola, M.; Baudys, M.; Zazpe, R.; Krbal, M.; Michalicka, J.; Rodriguez-Pereira, J.; Pavlinak, D.; Prikryl, J.; Hromadko, L.; Sopha, H.; Krýsa, J.; Macak, J. M. 2D MoS_2 nanosheets on 1D anodic TiO_2 nanotube layers: an efficient co-catalyst for liquid and gas phase photocatalysis. *Nanoscale* **2019**, *11*, 23126–23131.

(19) Zazpe, R.; Krumpolec, R.; Sopha, H.; Rodriguez-Pereira, J.; Charvot, J.; Hromadko, L.; Kolibalova, E.; Michalicka, J.; Pavlinak, D.; Motola, M.; Prikryl, J.; Krbal, M.; Bures, F.; Macak, J. M. Atomic Layer Deposition of $MoSe_2$ Nanosheets on TiO_2 Nanotube Arrays for Photocatalytic Dye Degradation and Electrocatalytic Hydrogen Evolution. *ACS Appl. Nano Mater.* **2020**, *3*, 12034–12045.

(20) Liu, K.-K.; Zhang, W.; Lee, Y.-H.; Lin, Y.-C.; Chang, M.-T.; Su, C.-Y.; Chang, C.-S.; Li, H.; Shi, Y.; Zhang, H.; Lai, C.-S.; Li, L.-J. Growth of Large-Area and Highly Crystalline MoS_2 Thin Layers on Insulating Substrates. *Nano Lett.* **2012**, *12*, 1538–1544.

(21) Hasani, A.; Le, Q. V.; Tekalgne, M.; Choi, M.-J.; Choi, S.; Lee, T. H.; Kim, H.; Ahn, S. H.; Jang, H. W.; Kim, S. Y. Fabrication of a WS_2/p-Si Heterostructure Photocathode Using Direct Hybrid Thermolysis. *ACS Appl. Mater. Interfaces* **2019**, *11*, 29910–29916.

(22) Moser, J.; Levy, F. Growth mechanisms and near-interface structure in relation to orientation of MoS_2 sputtered thin films. *Journal of Materials Research* **1992**, *7*, 734–740.

(23) Ohashi, T.; Suda, K.; Ishihara, S.; Sawamoto, N.; Yamaguchi, S.; Matsuura, K.; Kakushima, K.; Sugii, N.; Nishiyama, A.; Kataoka, Y.; Natori, K.; Tsutsui, K.; Iwai, H.;

Ogura, A.; Wakabayashi, H. Multi-layered MoS_2 film formed by high-temperature sputtering for enhancement-mode nMOSFETs. *Japanese Journal of Applied Physics* **2015**, *54*, 04DN08.

(24) Villamayor, M. M. S.; Lindblad, A.; Johansson, F. O.; Tran, T.; Pham, N. H.; Primetzhofer, D.; Sorgenfrei, N. L.; Giangrisotomi, E.; Fohlisch, A.; Lourenço, P.; Bernard, R.; Witkowski, N.; Prevot, G.; Nyberg, T. Growth of two-dimensional WS_2 thin films by reactive sputtering. *Vacuum* **2021**, *188*, 110205.

(25) Tao, J.; Chai, J.; Lu, X.; Wong, L. M.; Wong, T. I.; Pan, J.; Xiongb, Q.; Chi, D.; Wang, S. Growth of wafer-scale MoS_2 monolayer by magnetron sputtering. *Nanoscale* **2015**, *7*, 2497–2503.

(26) Pondick, J. V.; Woods, J. M.; Xing, J.; Zhou, Y.; Cha, J. J. Stepwise Sulfurization from MoO_3 to MoS_2 via Chemical Vapor Deposition. *ACS Appl. Nano Mater.* **2018**, *1*, 5655–5661.

(27) Huang, J.-H.; Hsu, H.-H.; Wang, D.; Lin, W.-T.; Cheng, C.-C.; Lee, Y.-J.; Hou, T.-H. Polymorphism Control of Layered $MoTe_2$ through Two-Dimensional Solid-Phase Crystallization. *Sci Rep* **2019**, *9*, 8810.

(28) Krbal, M. et al. Amorphous-to-Crystal Transition in Quasi-Two-Dimensional MoS_2: Implications for 2D Electronic Devices. *ACS Appl. Nano Mater.* **2021**, *4*, 8834–8844.

(29) Ravel, B.; Newville, M. ATHENA, ARTEMIS, HEPHAESTUS: data analysis for X-ray absorption spectroscopy using IFEFFIT. *J. Synchrotron Rad.* **2005**, *12*, 537–541.

(30) Whittingham, M. S.; Gamble Jr., F. R. The lithium intercalates of the transition metal dichalcogenides. *Mat. Res. Bull.* **1975**, *10*, 363–372.

(31) Kiessig, H. Untersuchungen zur Totalreflexion von Rontgenstrahlen. *Ann. Phys.* **1931**, *402*, 715–768.

(32) Simpson, R. E.; Fons, P.; Kolobov, A. V.; Krbal, M.; Tominaga, J. Enhanced crystallization of GeTe from an Sb_2Te_3template. *Appl. Phys. Lett.* **2012**, *100*, 021911.

(33) Wu, L.; Longo, A.; Dzade, N. Y.; Sharma, A.; Hendrix, M. R. M., Marco; Bol, A. A.; de Leeuw, N. H.; Hensen, E. J. M.; Hofmann, J. P. The Origin of High Activity of Amorphous MoS_2 in the Hydrogen Evolution Reaction. *ChemSusChem* **2019**, *12*, 4383–4389.

(34) Lassalle-Kaiser, B.; Merki, D.; Vrubel, H.; Gul, S.; Yachandra, V. K.; Hu, X.; Yano, J. Evidence from in Situ X-ray Absorption Spectroscopy for the Involvement of Terminal Disulfide in the Reduction of Protons by an Amorphous Molybdenum Sulfide Electrocatalyst. *J.Am.Chem.Soc.* **2015**, *137*, 314–321.

(35) Cramer, S.; Liang, K.; Jacobson, A.; Chang, C. H.; Chianelli, R. EXAFS studies of amorphous molybdenum and tungsten trisulfides and triselenides. *Inorganic Chemistry* **1984**, *23*, 1215–1221.

(36) Youn, D. H.; Jang, J.-W.; Kim, J. Y.; Jang, J. S.; Choi, S. H.; Lee, J. S. Fabrication of graphene-based electrode in less than a minute through hybrid microwave annealing. *Scientific Reports* **2014**, *4*, 5492.

(37) Yoo, H. D.; Li, Y.; Liang, Y.; Lan, Y.; Wang, F.; Yao, Y. Intercalation Pseudocapacitance of Exfoliated Molybdenum Disulfide for Ultrafast Energy Storage. *ChemNanoMat* **2016**, *2*, 688–691.

(38) Mondal, A.; Paul, A.; Srivastava, D. N.; Panda, A. B. Defect- and Phase-Induced Acceleration of Electrocatalytic Hydrogen Production by Ultrathin and Small MoS_2-Decorated rGO Sheets. *ACS Appl. Nano Mater.* **2018**, *1*, 4622–4632.

(39) Fleisch, T. H.; Mains, G. J. An XPS study of the UV reduction and photochromism of MoO_3 and WO_3. *J. Chem. Phys.* **1982**, *76*, 780.

(40) Gandubert, A. D.; Legens, C.; Guillaume, D.; Payen, E. X-ray photoelectron spectroscopy surfacequantification of sulfided CoMoP catalysts. Relationbetween activity and promoted sites. Part II: Influenceof the sulfidation temperature. *Surf. Interface Anal.* **2006**, *38*, 206–209.

(41) Lin, C.-H.; Tsai, C.-H.; Tseng, F.-G.; Yu, Y.-Y.; Wu, H.-C.; Hsieh, C.-K. Low-Temperature Thermally Reduced Molybdenum Disulfide as a Pt-Free Counter Electrode for Dye-Sensitized Solar Cells. *Nanoscale Research Letters* **2015**, *10*, 446.

(42) Eda, G.; Yamaguchi, H.; Voiry, D.; Fujita, T.; Chen, M.; Chhowalla, M. Photoluminescence from Chemically Exfoliated MoS_2. *Nano Lett.* **2011**, *11*, 5111–5116.

(43) Zhang, Y.; Kuwahara, Y.; Mori, K.; Yamashita, H. Defect Engineering of MoS_2 and Its Impacts on Electrocatalytic and Photocatalytic Behavior in Hydrogen Evolution Reactions. *Chem. Asian J.* **2021**, *14*, 278–285.

(44) Bradford, J.; Zaganelli, A.; Qi, D.; Zebardastan, N.; Shafiei, M.; MacLeod, J.; Motta, N. Substrate-mediated growth of oriented, vertically aligned MoS_2 nanosheets on vicinal and on-axis SiC substrates. *Applied Surface Science* **2021**, *552*, 149303.

(45) Smart, R. S. C.; Skinner, W. M.; Gerson, A. R. XPS of sulphide mineral surfaces: metal-deficient, polysulphides, defects and elemental sulphur. *Surf. Interface Anal.* **1999**, *28*, 101–105.

(46) Chen, C. P.; Ong, B. L.; Ong, S. W.; Ong, W.; Tan, H. R.; Chai, J. W.; Zhang, Z.; Wang, S. J.; Pan, J. S.; Harrison, L. J.; Kang, H. C.; Tok, E. S. In-situ growth of HfO_2 on clean 2H-MoS_2 surface: Growth mode, interface reactions and energy band alignment. *Appl. Surf. Sci* **2017**, *420*, 523–534.

(47) Hansen, L. P.; Johnson, E.; Brorson, M.; Helveg, S. Growth Mechanism for Single- and Multi-Layer MoS_2 Nanocrystals. *J. Phys. Chem. C* **2014**, *118*, 22768–22773.

For Table of Contents Use Only

Improved Ordering of Quasi-Two-Dimensional MoS_2 via an Amorphous-to-Crystal Transition Initiated from Amorphous Sulfur-rich MoS_{2+x}

Milos Krbal*, Vit Prokop, Jan Prikryl, Jhonatan Rodriguez Pereira, Igor Pis, Alexander V. Kolobov, Paul J. Fons, Yuta Saito, Shogo Hatayama, Yuji Sutou

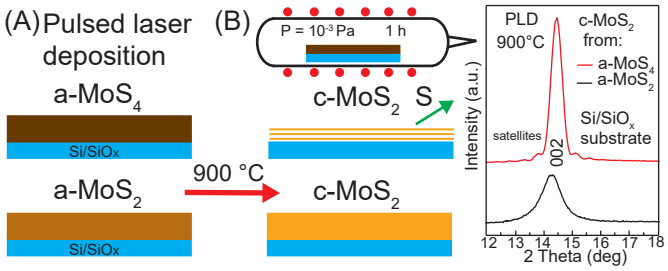

The arrangement of the MoS_2 layers is improved by the crystallization of an amorphous Sulfur-rich MoS_{2+x} thin film.